IOP PUBLISHING JOURNAL OF OPTICS
J. Opt. **14** (2012) 114003 (7pp) doi:10.1088/2040-8978/14/11/114003

Phase conjugation metamaterials: particle design and imaging experiments

A R Katko[1], G Shvets[2] and S A Cummer[1]

[1] Department of Electrical and Computer Engineering and Center for Metamaterials and Integrated Plasmonics, Duke University, Durham, NC 27708, USA
[2] Department of Physics, The University of Texas at Austin, Austin, TX 78712, USA

E-mail: cummer@ee.duke.edu

Received 15 February 2012, accepted for publication 29 March 2012
Published 27 July 2012
Online at stacks.iop.org/JOpt/14/114003

Abstract
We present simulation and experimental results demonstrating the effectiveness of phase conjugation or, equivalently, time reversal metamaterials for imaging applications. Split-ring resonators are loaded with varactor diodes to enable straightforward, easy-to-fabricate phase conjugation metamaterial unit cells. These cells are improved upon to allow either completely wireless operation or more efficient phase conjugate signal generation through the use of active loading elements. The metamaterials are demonstrated experimentally to produce time reversed signals with useful properties. An array of metamaterial cells is then constructed and shown to act as a negatively refracting imaging system.

Keywords: metamaterials, nonlinear metamaterials, phase conjugation, time reversal

(Some figures may appear in colour only in the online journal)

1. Introduction

Metamaterials are composites designed such that the electromagnetic properties of the composite structure are different from those of the constituent materials. The effective properties of the structure can be designed such that it mimics naturally occurring materials but with very different mechanical properties [1] or such that it exhibits properties not found in natural materials [2]. In recent years considerable effort has been expended towards designing functional metamaterials with interesting and unusual properties such as nonreciprocity [3], loss compensation [4], and mixing of waves [5].

Time reversal or phase conjugation metamaterials make up a particularly interesting class of nonlinear functional metamaterials. Time reversal has been used for a variety of applications. Time reversal media are used for applications such as holography [6], retrodirective arrays in the microwave regime [7], and slow light in the optical regime [8]. Time reversal elements are also used in acoustic applications such as propagation through random media or inverse problems [9]. These applications can be enabled by signal processing (in the microwave or acoustic regimes) [9], mixing circuitry [10], or four-wave mixing (in the optical regime) [6]. The dynamics of nondegenerate four-wave mixing, including phase mismatch, have also been studied with applications for photorefractive oscillators [11].

Phase conjugation (PC) is equivalent to time reversal over a finite bandwidth. We previously demonstrated [12] that nonlinear parametric pumping can be used to create a negatively refracting, phase conjugating metamaterial. Such phase conjugation media can be used for applications including negative refraction [12], four-wave mixing imaging [13], subwavelength resolution using near field to far field converting scatterers [10], and subwavelength antenna arrays exploiting subwavelength resolution [14].

In our previous work on this topic [12] we demonstrated negative refraction with PC metamaterials. The work was limited, however, by low PC signal generation due to inefficient elements and the small array size of PC metamaterials. We demonstrated negative refraction but the small array and inefficient metamaterial elements were unable to accurately image a source. In this work we demonstrate how PC metamaterials can be used to realize imaging systems. We also demonstrate that PC metamaterials can be made significantly more efficient and completely wireless, leading

to simple and practical implementations of PC systems. We design new all-wireless elements and more efficient PC metamaterial elements, including an active unit cell allowing loss compensation. We verify the functionality of these new PC metamaterials through both simulations and experiments. We also demonstrate the effectiveness of PC metamaterials for conducting imaging through both simulations and experiments.

2. PC metamaterial unit cells and wireless pumping

2.1. Unit cell design

It was demonstrated in [12] that a parametrically pumped resonant metamaterial produces a PC signal. The basic unit cell design considered in this work is a metamaterial loaded with a nonlinear, voltage-dependent capacitance. The metamaterial is excited by a pump signal and an illumination signal, also called a source signal. The equation characterizing the dipole moment of such a metamaterial excited by an incident wave at a frequency ω_1 is [12]

$$\frac{\mathrm{d}^2 p_j}{\mathrm{d}t^2} + \gamma \frac{\mathrm{d}p_j}{\mathrm{d}t} + \Omega_0^2(1 + h_0 \sin(2\omega_0 t))p_j = \sum_{k_y} \Omega_0^2 E(k_y) a^3 \mathrm{e}^{-\mathrm{i}(\omega_1 t - k_y y_j)} + \text{c.c.}. \quad (1)$$

Here p_j is the induced dipole moment of an individual metamaterial unit cell, γ is the loss rate, Ω_0 is the natural resonant frequency of the metamaterial unit cell, h_0 is the strength of the pump signal, ω_0 is the frequency of the pump signal, and y_j is the location of an individual metamaterial unit cell. $E(k_y)$ is the electric field for each spatial wavenumber and a is the effective size of the metamaterial unit cell. One solution of this equation for such a nonlinear metamaterial has the form of $\exp(\mathrm{i}\omega_2 t)$, where $\omega_2 = 2\omega_0 - \omega_1$, while the other solution has the form of $\exp(-\mathrm{i}\omega_1 t)$. The solution proportional to $\exp(\mathrm{i}\omega_2 t)$ (the mixed signal at the difference frequency) is a phase conjugate signal. The amplitude of this signal is maximized when the following conditions are met (where Ω_0 is the natural resonant frequency of the metamaterial without any pump signal applied):

$$\omega_0 = \Omega_0 \quad (2)$$

$$\omega_1 = \omega_0. \quad (3)$$

This is the degenerate frequency case, so-called because the PC signal will be produced at $\omega_2 = 2\omega_0 - \omega_0 = \omega_0$. However, this is very difficult to measure experimentally because the generated PC signal is lower in magnitude than the illumination signal. If the nondegenerate frequency case applies the magnitude of the PC signal will be lower but more easily detected.

We choose the frequencies of interest first. The PC signal frequency f_{PC} was chosen to be within the ISM band. The ISM band near 900 MHz is a frequency band set aside for non-communication industrial, scientific, and medical purposes and is free of local external interference. Discrete varactor diodes such as the ones considered here typically have a capacitance of approximately 1 pF (dependent on bias) and a lead inductance of approximately 1.5 nH. Such varactor diodes have a self-resonant frequency of 4.1 GHz. Thus, operation near this frequency range or above results in substantially different characteristics of the varactor diodes. Higher frequency operation requires smaller capacitances and parasitic inductances. Such requirements could be met by on-chip devices, but very high frequency PC metamaterials using similar diodes to those examined here are constrained to lower frequency bands. The chosen f_{PC} is far enough from the self-resonant frequency that the varactor can be treated as a simple voltage-dependent capacitance. In order to avoid local interferers the source frequency was set at 950 MHz and the pump frequency was set at 1850 MHz.

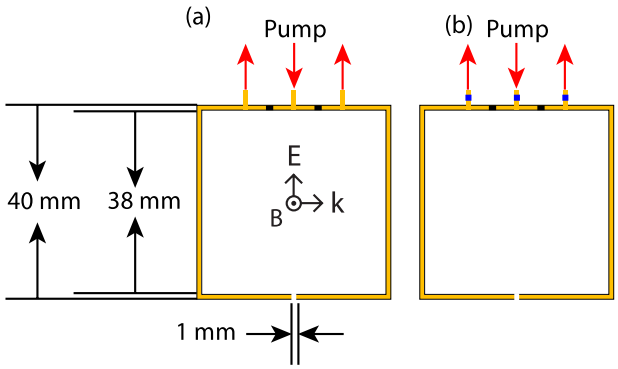

Figure 1. Schematic of PC SRR design. Black rectangles are the varactor diodes. Dimensions are shown along with signal paths and polarization. The signal path for the pump leads to a direct cable connection with an SMA adaptor. (a) The simple RF connected element. (b) The simple RF connected element with matching network.

We begin with the canonical metamaterial structure, the split-ring resonator (SRR). It was shown [12] that if the resonant frequency of a nonlinear metamaterial is varied parametrically one of the generated signals is PC. We implement this using a nonlinear lumped device loaded into the SRR. A Skyworks SMV1405 varactor diode was chosen to provide the nonlinear behavior. The varactor diode's capacitance varies with reverse bias voltage from 0.63 to 2.67 V. The amplitude of the PC signal depends upon the relationship between the pump, source, and natural resonant frequencies. For a strong PC signal the PC frequency and source frequency should be close to the natural resonant frequency of the metamaterial. The SRR is designed to resonate near f_{source} to meet this criterion. The simple SRR is shown in figure 1(a). The PC signal produced by this very simple element is fairly low in amplitude, however. A simple matching network was used to increase the power across the varactor diodes. Inductors were inserted along the pump signal path to provide this matching. The revised PC SRR is shown in figure 1(b). The matching inductors were used in all other elements detailed here.

This basic PC SRR is straightforward to fabricate and operate. A direct cable connection to the SMA adaptor is required to provide the pump signal. The PC signal amplitude depends upon the modulation of the resonant frequency of the

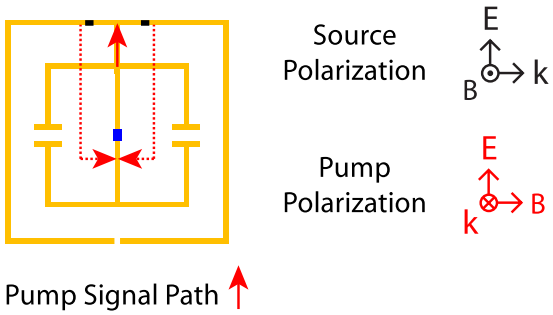

Figure 2. Schematic of the wireless metamaterial design. Black rectangles are the varactor diodes. The blue rectangle provides a load to harvest voltage from the ELC section. The pump signal path is shown by red arrows. The dashed arrows are on the underside of the dielectric using vias. Appropriate polarizations for the source and pump are shown.

metamaterial, which is determined by the capacitance of the varactor diodes. The varactor diode capacitance is modulated by the pump signal voltage. A large PC signal amplitude requires a large modulation of the resonant frequency of the metamaterial and thus a large pump signal voltage. The pump signal amplitude is maximized by direct cable connections, allowing no free space path loss for the signal. The direct cable connection utilized with the simple PC SRR results in a large PC signal amplitude. However, for large-scale operation, many direct coaxial cable connections are impractical. Ideal operation of the PC metamaterial also requires that the pump signal at each metamaterial unit cell is in phase. Many direct cable connections introduce small phase variations to individual unit cells, which inhibits the performance of the PC metamaterial.

We design another version of the PC metamaterial to counteract these disadvantages. Using a purely wireless metamaterial unit cell we can predict the phase at each unit cell with high accuracy as long as far field conditions hold, and the numerous direct cable connections and power dividers are no longer needed. We modified the metamaterial to include two sections. The first section is the base SRR, which couples to the source signal, includes the varactors for generating the PC signal, and re-radiates at the PC frequency (which is generally close to both the source frequency and resonant frequency of the SRR). The second section is designed to couple to the pump signal and provide a bias voltage across the varactors. We choose to use an electric inductive–capacitive (ELC) resonator for the second section as it provides a low-profile and electrically small design. The two sections are coplanar and are simply connected, as shown in figure 2.

The unit cell shown in figure 2 allows the use of a wireless pump signal. This topology was also chosen to allow insertion of other devices and functions between the ELC section and the SRR section. This could include a matching network, bandpass filters, or active circuitry. We investigate the addition of a simple amplifier network embedded in each particle between the ELC section and the SRR section. The use of a completely wireless pump decreases the possible signal level at the metamaterial due to free space path loss and impedance mismatches (including a possible mismatch between the ELC section and the SRR section). This topology allows the addition of active elements between the metamaterial sections which can compensate for the signal loss. A simple amplifier and bias network does add wired connections to the unit cells. However, these connections are simply DC bias lines rather than RF signal lines, so the issue of phase error in the pump signal is not present. Thus we investigate three versions of the PC metamaterial. The first is the simple unit cell with direct RF cable connections. The second is an entirely passive, all-wireless unit cell. The third is an active unit cell with only DC bias connections. Photographs of the three metamaterials under investigation are shown in figure 3. Simulations were used to validate the designs of the simple and wireless PC metamaterials. These simulations will be discussed in the following section.

2.2. Nonlinear circuit simulations

First LTSpice was used to simulate a lumped-element circuit equivalent to the metamaterial unit cell. This simulation was used to verify the performance of the particular varactor diodes used in this work and show that the nonlinearity of the varactor diodes was sufficient for efficient PC signal generation.

The signal generation process of a resonator with a parametrically varying resonance is described by the following equation discussed earlier:

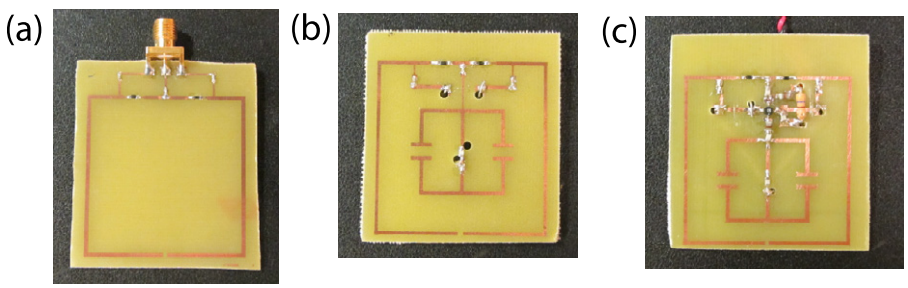

Figure 3. Photographs of fabricated PC metamaterials. (a) The simple direct RF connected metamaterial. (b) The passive, all-wireless metamaterial. (c) The active, DC bias connected metamaterial.

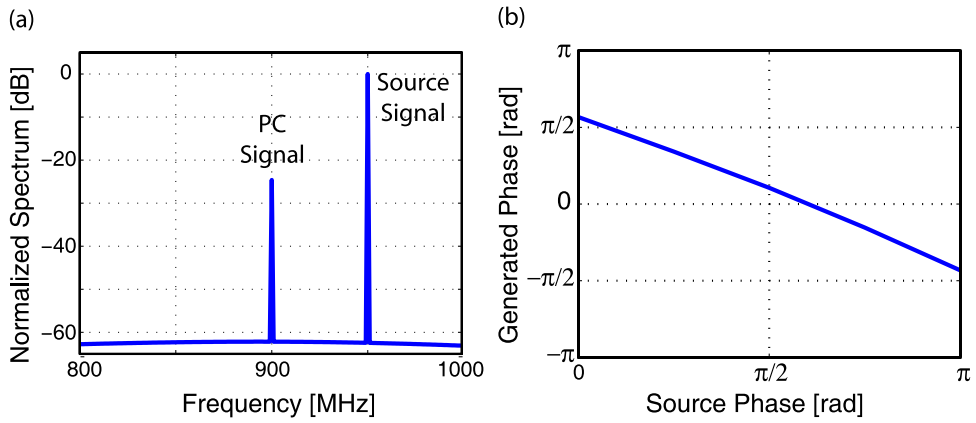

Figure 4. Numerical study of the mixing process. (a) Generated signal amplitude relative to the source signal. (b) Phase of the generated signal as a function of the source signal phase. A positive change in the source phase yields a negative change in the generated signal phase, indicating that the generated signal is PC.

$$\frac{\mathrm{d}^2 p_j}{\mathrm{d}t^2} + \gamma \frac{\mathrm{d}p_j}{\mathrm{d}t} + \Omega_0^2(1 + h_0 \sin(2\omega_0 t))p_j = \sum_{k_y} \Omega_0^2 E(k_y) a^3 \mathrm{e}^{-\mathrm{i}(\omega_1 t - k_y y_j)} + \text{c.c.}. \quad (4)$$

MATLAB was used to numerically solve this equation with a standard Runge–Kutta method. The solution was examined to test properties of the generated harmonics and examine whether phase conjugation was predicted numerically. An example result is shown in figure 4.

Figure 4(a) shows the calculated amplitude of the signal at the predicted PC harmonic (the difference frequency, $f_{\text{pump}} - f_{\text{source}}$). This signal was calculated for different values of the source signal phase. The generated signal was calculated for source phase values of $\phi_{\text{source}} = 0, \frac{\pi}{4}, \frac{\pi}{2}, \pi$. A PC signal should vary as $-\phi_{\text{source}}$ and this is indeed what is observed in figure 4(b).

2.3. Experiments and discussion

The wireless PC metamaterial unit cells are also tested to verify their functionality. The pump signal generator is connected to an antenna and a spectrum analyzer is used to record the generated signal from both the wireless metamaterial unit cells. Each unit cell is tested individually with the same geometric arrangement and signal levels. To establish a baseline for external interference, the spectrum of interest (800–1000 MHz) is recorded with all of our signals shut off. Signal generators are used for the source and pump signals. The measured 3 dB bandwidths for these two signals are 1.4 kHz (for the source) and 2.0 kHz (for the pump). We record the spectrum when each of the three PC metamaterials are excited individually to record the strength of the generated PC signal.

The 3 dB bandwidths for the PC signal generated by each metamaterial were 1.2 kHz (for the simple RF connected metamaterial), 1.8 kHz (for the all-wireless metamaterial), and 1.4 kHz (for the active metamaterial). Thus, the elements are not significantly modifying the signal bandwidths from those generated by the source and the pump. After measuring the signal bandwidths we decreased the resolution of the spectrum analyzer, allowing easier data collection, processing, and examination.

The measured signals are then normalized to the source signal. The measured data are shown in figure 5. In figure 5(a) the data are normalized to the measured source signal in order to show the full spectrum. In figure 5(b) the data are normalized to the source signal incident at the metamaterial in order to determine the efficiency of the PC signal generation.

These measurements show that the three PC metamaterials all generate a strong, measurable signal at 900 MHz. The simple RF connected metamaterial produces a signal 26 dB below the incident source signal. This metamaterial is suitable for applications requiring relatively small metamaterial arrays or few individual elements, or applications requiring extremely strong PC signal generation. The all-wireless metamaterial produces a signal 59 dB below the incident source signal. While lower than the RF connected metamaterial, this is still easily detectable above noise. This metamaterial is suitable for non-invasive applications or applications requiring large-scale PC metamaterials. The active metamaterial produces a signal 36 dB below the incident source signal. The inclusion of active elements compensates for the free space path loss due to using a wireless pump signal and impedance mismatch losses. The active metamaterial is suitable for applications requiring very strong PC signal generation on a large scale.

3. PC metamaterial imaging

Having demonstrated that individual PC metamaterial unit cells can be used for phase conjugation, the possibility of practical imaging using PC metamaterials is investigated. For this work the simple RF connected metamaterials are used in order to produce the maximum PC signal level. An array of eight simple RF connected PC metamaterials is considered. Simulations using COMSOL Multiphysics are conducted to predict the imaging performance of an array of PC metamaterials. Experiments are then used to validate

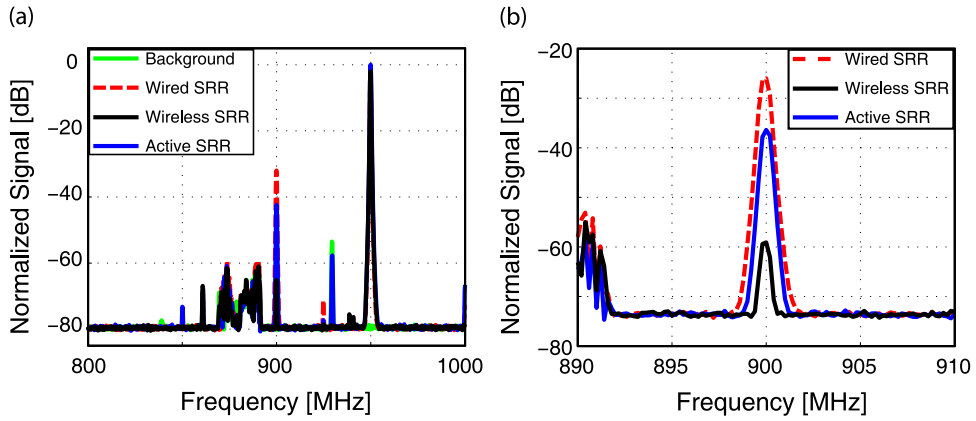

Figure 5. Measured spectra for four cases. Solid green is background signal levels (no equipment on). Dashed red is the simple RF connected metamaterial. Solid black is the all-wireless metamaterial. Solid blue is the active metamaterial. (a) Full measured spectrum normalized to the source signal (at 950 MHz). (b) Zoom on the PC signal normalized to the incident source signal to determine PC signal generation efficiency.

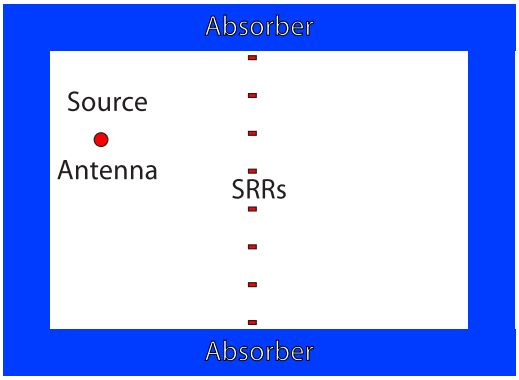

Figure 6. Geometry considered both for COMSOL simulations and imaging experiments. The eight SRRs form an array in the center of the domain, spaced 0.75 wavelengths apart. An absorber is used as a PML in simulations and to reduce the effects of external scatterers and interference in the experiments.

the simulation results and demonstrate the effectiveness of imaging using PC metamaterials.

3.1. Simulations

We conduct simulations using COMSOL Multiphysics to verify the setup of the imaging experiment. We consider a two-dimensional imaging experiment with an antenna exciting individual PC metamaterial unit cells. COMSOL is used to simulate the generated field from the PC metamaterial. This simulation takes into account nonideal factors in the imaging performance, including the nondegenerate frequency case ($f_{PC} \neq f_{source}$) and the actual radiation pattern of the PC metamaterials. As a very thin slab of PC medium, the reradiated pattern is symmetric about the slab [15]. An array of eight discrete metamaterial unit cells is considered, with a source excitation located three wavelengths normal to the array and one wavelength from the center of the array. A diagram of the geometry considered is shown in figure 6.

The produced fields from both the source alone and the PC metamaterial using COMSOL are shown in figure 7.

The image spots (both forward and backward) are denoted in the figure. Other local extrema are sidelobes from the array. The simulations show that a discrete PC metamaterial will produce a clearly distinguishable image spot, denoted in the figure. There is substantial distortion very close to the metamaterial, so imaging is only feasible a few wavelengths away from the metamaterial.

3.2. Experiments and discussion

We describe experimental verification of the PC metamaterial imaging functionality. We demonstrated that the simple PC metamaterials accomplished PC and negative refraction (but not imaging) in [12]. We demonstrate imaging using simple PC metamaterials with a simple but effective experiment in this work. An array of eight unit cells was constructed to form our PC metamaterial. Signal generators were used to act as the pump and source. The simple unit cells were used for this experiment so the pump was directly connected to each unit cell, while a monopole antenna over a ground plane was used for the source. Microwave absorbers were used to construct a two-dimensional test bed without external scatterer interference. The source antenna was positioned in multiple locations to demonstrate the negatively refracting imaging of the PC metamaterial. The first measurement is conducted for the source positioned 3λ from the PC metamaterial (normal) and centered along the axis of the PC metamaterial. The measurements are compared to simulations in figure 8.

As shown in figure 8 the measured image spot is in approximately the location predicted by simulation. The distortion close to the metamaterial is predicted by simulation, demonstrating a minimum effective imaging distance. In order to demonstrate the negatively refracting imaging ability of this PC metamaterial, the source was moved off-axis from the metamaterial. The simulated and measured results are shown in figure 9.

These results clearly demonstrate that the PC metamaterial is effective for imaging, even with an array of only eight unit cells, in a straightforward manner.

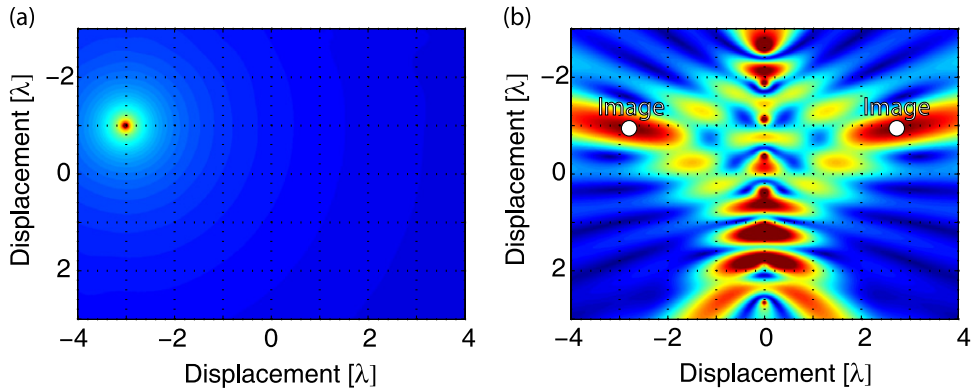

Figure 7. COMSOL Multiphysics simulations of the imaging experiment. (a) The field produced by the source antenna alone. The position is $(-3, -1)$ wavelengths from the center of the domain. (b) The field produced by the discrete PC metamaterial. The metamaterial cells are positioned along the *y*-axis. The white circles are the image spots produced by the PC metamaterial. Note that the image spots are in approximately the same location in (b) as the source in (a), both forward and backward.

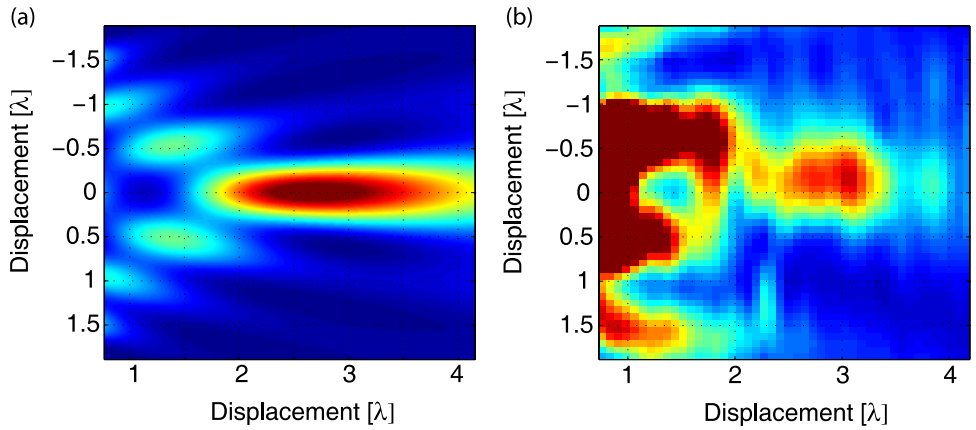

Figure 8. Simulated and measured field patterns for the centered source experiment. (a) Simulated normalized $|E|$, with the scale in wavelengths. (b) Measured normalized $|E|$, with the scale in wavelengths.

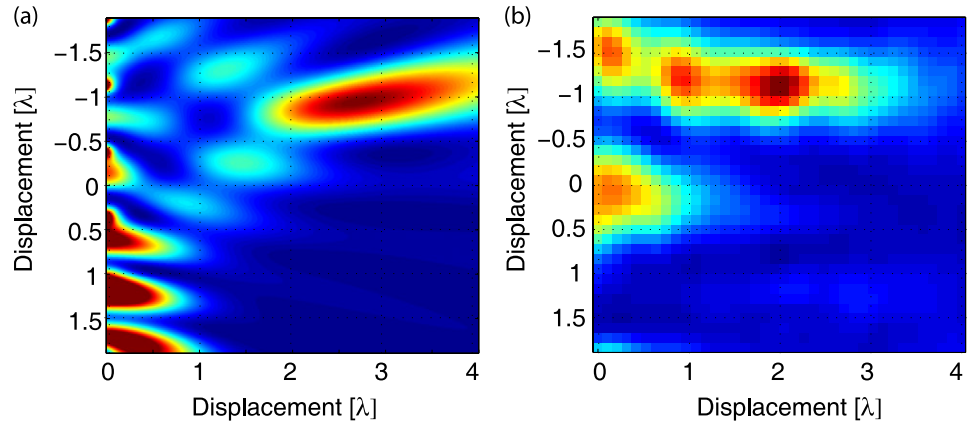

Figure 9. Simulated and measured field patterns for the off-axis source experiment. (a) Simulated normalized $|E|$, with the scale in wavelengths. (b) Measured normalized $|E|$, with the scale in wavelengths.

4. Conclusions

We have demonstrated that PC metamaterials can be used for effective imaging. The imaging ability of PC metamaterials was verified through both simulations and experiments. COMSOL Multiphysics was used to simulate imaging with a finite array of PC metamaterial unit cells and the results were validated experimentally. Moreover, other, more practical PC metamaterial unit cells were also investigated. The performance of both all-wireless and active, DC bias connected PC metamaterials was demonstrated experimentally. All-wireless PC metamaterials allow phase

conjugation without any direct connections, allowing non-invasive negative refraction imaging. Active PC metamaterials with only DC bias lines were demonstrated, compensating for loss of signal strength due to the use of a wireless pump. These results demonstrate the promise of using PC metamaterials for a variety of applications requiring retrodirectivity, imaging, or negative refraction.

Acknowledgments

This work was supported by a Multidisciplinary University Research Initiative from the Army Research Office (contract no. W911NF-09-1-0539) and by a Lockheed Martin University Research Initiative. The authors wish to thank Allen Hawkes for assistance.

References

[1] Pendry J B, Holden A J, Robbins D J and Stewart W J 1999 Magnetism from conductors and enhanced nonlinear phenomena *IEEE Trans. Microw. Theory Tech.* **47** 2075–84
[2] Smith D R, Padilla W J, Vier D C, Nemat-Nasser S C and Schultz S 2000 Composite medium with simultaneously negative permeability and permittivity *Phys. Rev. Lett.* **84** 4184–7
[3] Shadrivov I V, Fedotov V A, Powell D A, Kivshar Y S and Zheludev N I 2011 Electromagnetic wave analogue of an electronic diode *New J. Phys.* **13** 033025
[4] Yuan Y, Popa B-I and Cummer S A 2009 Zero loss magnetic metamaterials using powered active unit cells *Opt. Express* **17** 16135–43
[5] Huang D, Rose A, Poutrina E, Larouche S and Smith D R 2011 Wave mixing in nonlinear magnetic metacrystal *Appl. Phys. Lett.* **98** 204102
[6] Yariv A 1978 Phase conjugate optics and real-time holography *IEEE J. Quantum Electron.* **14** 650–60
[7] Chiu L, Yum T Y, Chang W S, Xue Q and Chan C H 2006 Retrodirective array for rfid and microwave tracking beacon applications *Microw. Opt. Technol. Lett.* **48** 409–11
[8] Mathey P, Gadret G and Shcherbin K 2011 Slow light with degenerate backward-wave four-wave mixing *Appl. Phys.* B **102** 539–43
[9] Fink M and Prada C 2001 Acoustic time-reversal mirrors *Inverse Problems* **17** R1–R38
[10] Malyuskin O and Fusco V 2010 Far field subwavelength source resolution using phase conjugating lens assisted with evanescent-to-propagating spectrum conversion *IEEE Trans. Antennas Propag.* **58** 459–68
[11] Rebhi R, Mathey P, Jauslin H-R, Cook G, Evans D and Odoulov S 2009 Dynamics of four wave mixing oscillators with quasi phase matching *Phys. Rev.* A **80** 013803
[12] Katko A R, Gu S, Barrett J P, Popa B-I, Shvets G and Cummer S A 2010 Phase conjugation and negative refraction using nonlinear active metamaterials *Phys. Rev. Lett.* **105** 123905
[13] Palomba S, Zhang S, Park Y, Bartal G, Yin X and Zhang X 2012 Optical negative refraction by four-wave mixing in thin metallic nanostructures *Nature Mater.* **11** 34–8
[14] Ge G-D, Wang B-Z, Wang D, Zhao D and Ding S 2011 Subwavelength array of planar monopoles with complementary split rings based on far-field time reversal *IEEE Trans. Antennas Propag.* **59** 4345–50
[15] Pendry J B 2008 Time reversal and negative refraction *Science* **322** 71–3